In situ structural analysis of the flagellum attachment zone in *Trypanosoma brucei* using cryo-scanning transmission electron tomography

Sylvain Trépout

Institut Curie, Inserm US43, CNRS UMS2016, Université Paris-Sud, Université Paris-Saclay, Centre Universitaire, Bât. 101B-110-111-112, Rue Henri Becquerel, CS 90030, 91401 ORSAY Cedex, FRANCE

Email address: sylvain.trepout@curie.fr

Summary

The flagellum of *Trypanosoma brucei* is a 20 µm-long organelle responsible for locomotion and cell morphogenesis. The flagellum attachment zone (FAZ) is a multi-protein complex whose function is to attach the flagellum to the cell body but also to guide cytokinesis. Cryo-transmission electron microscopy is a tool of choice to access the close-to-native structure of the FAZ. However, because of the large dimension of the cell body, the whole FAZ cannot be structurally studied *in situ* at high resolution in 3D using classical transmission electron microscopy approaches. In the present work, cryo-scanning transmission electron tomography, a new method capable of investigating thick cryo-fixed biological samples, has been used to study the structure and organisation of whole *T. brucei* cells at the bloodstream stage. The method allowed to visualise intracellular structures located deep inside the cells such as the nucleus and the nuclear envelope and to localise nuclear pore complexes. The organisation of the stick-like structure of the macromolecular protein complexes composing the FAZ filament is depicted from the posterior part to the anterior tip of the cell. This study provides new insights in the structure the FAZ filament.

Keywords

Electron cryo-scanning transmission electron tomography, trypanosome, bloodstream forms, flagellum, flagellum attachment zone (FAZ), FAZ filament

Highlights

- Flagellar and cellular membranes are in close contact next to the FAZ filament
- Sticks are heterogeneously distributed along the FAZ filament length
- Thin appendages connect the FAZ filament sticks to neighbouring microtubules

Abbreviations

Transmission Electron Tomography (TET); Transmission Electron Microscopy (TEM); Scanning Transmission Electron Microscopy (STEM); Scanning Transmission Electron Tomography (STET); Flagellum Attachment Zone (FAZ)

Introduction

Trypanosoma brucei is a unicellular parasite responsible for human African trypanosomiasis, also known as sleeping sickness, occurring in sub-Saharan Africa (Büscher et al., 2017; Rotureau and Van Den Abbeele, 2013). This organism adopts different stages whose shape, intracellular organisation and metabolism vary during the complex life cycle in the insect vector or the mammalian host (bloodstream forms). Reverse genetic approaches such as RNA interference (Ngô et al., 1998), *in situ* tagging (Dean et al., 2015) and more recently CRISPR-Cas9 (Beneke et al., 2017) technologies are potent genetic tools to study gene function of fully sequenced *T. brucei* genome (Berriman et al., 2005; Sistrom et al., 2014). Furthermore, it has a single flagellum during the cell cycle except during cell duplication where a new flagellum (*i.e.* the one of the future daughter cell) is built next to the existing one (Lacomble et al., 2010, 2009; Sherwin and Gull, 1989). Mature cells have a single fully-grown 20 µm-long flagellum. The presence of a single flagellum is an advantage for the study of proteins present in the flagellum, making the phenotype of the inducible mutant cells more easily visible and distinctive than in multiflagellated cells (Blisnick et al., 2014). In *T. brucei*, the flagellum is responsible for cell locomotion (Bastin et al., 1998) and morphogenesis (Kohl et al., 2003). Mechanistically, it has been proposed that the bi-helical swimming pattern of *T. brucei* originates from flagellum motility which is transmitted to the cell body through a succession of structural connecting elements (Heddergott et al., 2012). The sliding model explaining flagellum motility has been first proposed by Peter Satir in 1968 (Satir, 1968). Since then, high resolution cryo-transmission electron microscopy (TEM) revealed that it originates from the force exerted by the outer and inner dynein arms on the 9 microtubules doublets of the axoneme (Lin et al., 2014; Lin and Nicastro, 2018). In the case of trypanosomes, the movement of the axoneme is then transmitted to the paraflagellar rod (PFR), a semi-crystalline multiprotein complex which is a unique feature of most species of the Kinetoplastid order among other eukaryotes (Koyfman et al., 2011; Vickerman, 1962). The PFR faces axonemal microtubules doublets 4 to 7 and makes several connections with the axoneme. In particular, a thick fibre connects microtubule doublet 7 to the PFR (Sherwin and Gull, 1989). A further contact located between the PFR and the flagellar membrane towards the cell body has also been identified (Sherwin and Gull, 1989). The flagellum attachment zone (FAZ) is a large macromolecular structure located at the cellular membrane facing the flagellum. It is composed of a filament spanning the cellular and flagellar membranes, a set a four microtubules called the microtubule quartet and a FAZ-associated reticulum. The FAZ filament is not present in regions in which the flagellum is intracellular (*i.e.* the flagellar pocket zone). It starts after the collar, which delimits the intracellular localisation of the flagellum, and ends at the cell body anterior end. The FAZ interdigitates between subpellicular microtubules which are forming an array below the cellular membrane of *T. brucei*. In mature cells, it is present along the whole interface between the flagellum and the cell body. The FAZ, and more particularly the FAZ filament is viewed as a main connecting element with a strong implication in the transfer of flagellum motility to the cell body.

Important knowledge on the FAZ filament composition has been collected from immunoprecipitation, immunofluorescence and bioinformatics (Hu et al., 2015; McAllaster et al., 2015; Moreira et al., 2017; Morriswood et al., 2013; Rotureau et al., 2014; Sunter et al., 2015; Vaughan et al., 2008; Zhou et al., 2015, 2011). The localisation of known FAZ filament proteins and a putative model of their interaction have been presented (Sunter and Gull, 2016). Proteins FAZ1 to FAZ3, FAZ5, FAZ8 to FAZ10 and CC2D localise along the FAZ filament whereas others proteins such as FAZ4, FAZ6, FAZ7, FAZ12 to FAZ14, TbSAS4 and TOEFAZ1 localise to the distal tip of the filament only. Using fluorescence, it has been shown that FAZ11 mainly localises at the FAZ filament distal tip but also possesses a dim localisation along the FAZ filament. Localisations of proteins FAZ15 to FAZ17 have not been identified yet. It has been proposed that the FAZ filament grows by proximal addition of proteins in either a "*push*" or a "*pull*" treadmill-like mechanism (Sunter and Gull, 2016). In the "*push*" model, the proximal addition of structural elements is thought to push the whole FAZ structure, whereas in the "*pull*" model a distal component, yet to be determined, is present in the flagellum compartment and is thought to pull the whole FAZ structure. The FAZ filament is a large macromolecular complex

whose structure has previously been investigated using electron microscopy, but not as extensively as other cytoskeletal elements such as the axoneme or the PFR. Indeed, classical TEM studies can only be used on thin specimens (< 250 nm) which is not compatible with the important size of the FAZ filament and its coiling around a micrometre-thick cell body. Several thinning strategies have been used to circumvent this issue: i) conventional resin sections (Sherwin and Gull, 1989), cryo-sections (Höög et al., 2012) and generation of thin anucleated mutant cells for global observation by cryo-TEM (Sun et al., 2018). The punctuated periodic structure of the FAZ filament has been visualised since the early studies on resin sections of heavy-metal stained cells and is also visible in some fluorescence images. First described as a mostly cytoplasmic filamentous structure (Sherwin and Gull, 1989) and later as extracellular staples (Höög et al., 2012), there are still some discrepancy in the understanding of the FAZ filament organisation and localisation. This observation might be explained by the lack of a systematic approach to study the FAZ filament since most structural studies were performed on thin sections where only a thin part of the FAZ filament could be observed.

Cryo-transmission electron tomography (cryo-TET) consists in the collection of projection images of a cryo-fixed sample tilted inside a transmission electron microscope (Frank, 2006). Projection images are then used to computationally reconstruct the object of interest in 3D. It is the method of choice to study macromolecular assemblies and cell components since it allows nanometric resolution imaging of a sample fixed in a close to native state (Lucic et al., 2013, 2008). Nevertheless, cryo-TET is limited to samples thinner than ~250 nm because of the strong proportion of inelastic scattering occurring in thicker samples (Aoyama et al., 2008). When the sample is too thick, it has to be thinned down using different means which can be cryo-sectioning (Höög et al., 2012). Alternatively, people have used smaller cells such as anucleated *T. brucei* (Sun et al., 2018). Scanning transmission electron microscopy (STEM) is an alternative imaging mode, it is based on a raster scanning of the electron beam that is focused on the sample, the transmitted electrons being collected by detectors (Midgley and Weyland, 2003; Pennycook and Nellist, 2011; Sousa and Leapman, 2012). There is no post-specimen electromagnetic lens in STEM and the image contrast only depends on amplitude contrast as opposed to TEM that relies on phase contrast. Thanks to these differences, STEM is more prone to image thicker samples (above 250nm) as compared to TEM (Aoyama et al., 2008). Furthermore, simulations have shown that micrometre-thick samples ("*and beyond*") could be studied using cryo-STET (Rez et al., 2016). However, only few studies have combined STEM tomography (STET) and cryo fixation to investigate the ultrastructure of biological specimens (Wolf et al., 2017, 2014). Nonetheless, cryo-STET appears as a promising approach to study cell components *in situ* in thick samples (Wolf and Elbaum, 2019). In the present work, cryo-STET has been applied to study the structure of the FAZ filament in whole chemically-immobilised and cryo-fixed *T. brucei* bloodstream cells. Tomographic reconstructions unveil that the FAZ filament is composed of an array of sticks which are heterogeneously distributed along its length. Furthermore, sticks are connected to neighbouring cytoplasmic microtubules via thin appendages whose length varies depending on the type of associated microtubule.

Material and methods

Sample preparation

T. brucei AnTat 1.1E bloodstream forms were cultivated in HMI-11 medium supplemented with 10% foetal calf serum at 37°C in 5% CO2. Exponential growth-phase cells ($2x10^6$ parasites/ml) were fixed with paraformaldehyde (4% w/w final concentration) directly in the culture medium. A 5 µl drop of the chemically fixed cell culture was deposited on a glow-discharged Quantifoil 200 mesh R2/2 electron microscopy grid (Quantifoil, Großlöbichau, Germany) pre-coated with gold beads. The grids were manually blotted using Whatman filter paper and plunge-frozen into liquid ethane at -174°C using a Leica EM-CPC equipment (Leica, Wetzlar, Germany). After freezing, the grids were stored in a liquid nitrogen tank until observation at the electron microscope.

Scanning transmission electron microscopy setup

Frozen electron microscopy grids were mounted on a Gatan 914 high-tilt cryo-holder (Gatan, Pleasanton, CA, USA). Cryo-STET dataset were collected on JEOL 2200FS 200kV field emission gun hybrid TEM/STEM electron microscope (JEOL, Tokyo, Japan). 3k by 3k images were collected using a JEOL bright-field STEM detector, at 60 cm camera length and 40 µm condenser aperture (beam convergence semi-angle and collection outer diameter were 9.3 and 6.6 mrad respectively). In a hybrid TEM/STEM instrument, the condenser aperture plays the role of the objective aperture in a dedicated STEM instrument. Dwell time was set to 1 µs/pixel and magnifications used ranged between 40,000x and 60,000x (corresponding pixel sizes ranged between 1.3 and 0.8 nm respectively). The analogic signal of the STEM detector was digitised to 16 bit values using a Digiscan II ADC (Gatan, Pleasanton, CA, USA).

Cryo-STET data acquisition

Images and tilt-series were collected in Digital Micrograph which is the user interface for controlling the Digiscan II. Digital Micrograph offers scripting possibilities to perform specific and redundant tasks in an automated way. Fully-automatic cryo-STET tilt-series were collected using a homemade script developed in Digital Micrograph. The STET acquisition software used here has been presented in details (Trépout, 2019). Briefly, focusing and tracking tasks are performed on a common region that is localised immediately next to the region of interest. This strategy allows to perform low-dose acquisition. Tilt-series were collected between -75° and +75° using 2° tilt increments. The total electron dose received by the sample was estimated at around 40 $e^-/Å^2$. In practice, the completion of a whole tilt-series acquisition consisting of ~70 images took ~90 minutes.

Image analysis and segmentation

Fiducial-based alignment and weighted back-projection reconstruction of the tilt-series were performed in Etomo (v.4.9.10) (Kremer et al., 1996; Mastronarde and Held, 2017). After reconstruction, 3D volumes were processed using an edge-enhancing noise-reduction anisotropic diffusion filter to enhance ultrastructural details typically using 10 to 20 iterations (Moreno et al., 2018). Exploration of the reconstructed volumes and segmentations were performed in semi-automatic mode using ImageJ (Schneider et al., 2012). Image measurements and statistical analysis were performed using Matlab (The MathWorks Inc., Natick, MA, USA). The movie was generated in Amira (ThermoFisher Scientific, Hillsboro, OR, USA).

Protein structure prediction and rendering

A set of 8 FAZ filament proteins (FAZ1 to FAZ3, FAZ5, FAZ8 to FAZ10 and CC2D) were submitted to Phyre2 (http://www.sbg.bio.ic.ac.uk/phyre2/html/page.cgi?id=index) for 3D structure prediction. Phyre2 structure prediction is based on protein homology (Kelley et al., 2015). Intensive modelling mode was used. FAZ10 is giant protein (0.5 MDa) that could not be modelled as a whole because of Phyre2 sequence size limitation. The FAZ10 protein sequence has then been divided into 5 segments of about 170 kDa each. Two consecutive segments shared an overlapping sequence of 85 kDa not to miss any potential domain prediction. FAZ filament protein structures predicted with high confidence (*i.e.* above 50% of the sequence modelled with more than 90% confidence) and that contained structural domains greater than 10 nm were rendered using ChimeraX (Goddard et al., 2018).

Results and discussion

Ultrastructural organisation of T. brucei

After immobilisation with paraformaldehyde, cells were deposited on electron microscopy grids, cryo-fixed in liquid ethane and imaged at the electron microscope. In cryo-tomograms, *T. brucei* bloodstream cells display the expected morphology and are embedded in amorphous ice (Fig. 1). In

some rare cases, the ice forms crystals and these regions are excluded from analyses (Fig. 1, white asterisks). The tomographic reconstruction contains the whole depth of the cell such that the entire nucleus is visible (Fig. 1A-C, N). The strong contrast allows the visualisation of the nucleolus which appears darker than the rest of the nucleus (Fig. 1A-B, white number sign). Furthermore, connections between the inner and the outer membranes of the nuclear envelope reveal the presence of nuclear pore complexes even at this relatively low magnification (Fig. 1B, yellow arrows). Details of the nuclear envelope are available in the magnified view (Fig. 1B, insert). The lysosome is detected on several slices of the reconstruction (Fig. 1A-C, L). In the posterior region of the cell body, a small part of the condensed DNA of *T. brucei* single mitochondrion called the kinetoplast (Fig. 1B, K) is visible next to the flagellar pocket (Fig. 1B, FP).

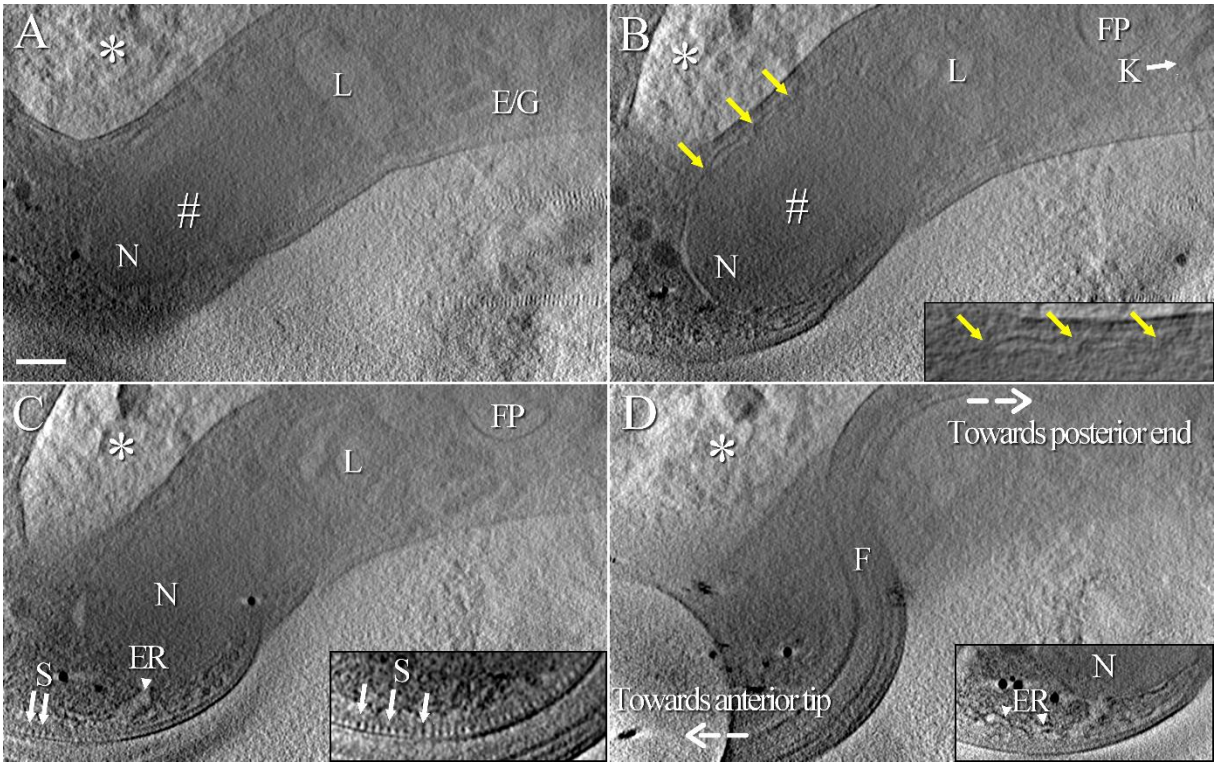

Figure 1. Ultrastructural organisation of a bloodstream *T. brucei* cell observed in cryo-STET. Each image is a 28 nm-thick slice made through a tomographic reconstruction, showing various structural elements found in *T. brucei*. A) Slice passing through the nucleus (N), the nucleolus (#), the lysosome (L) and some endosomes and/or glycosomes (E/G). B) On this second slice, the kinetoplast (K, white arrow), the flagellar pocket (FP) and the location of some nuclear pore complexes (yellow arrows) are visible. The insert is a close-up view of the nuclear envelope. C) Regularly-spaced stick-like dark densities (S, arrows) corresponding to the FAZ filament are located next to the FAZ-associated reticulum (ER, arrowhead). The insert is an oriented slice passing through the region of the FAZ filament in which the stick array (S) is visible on a larger scale. D) The last slice shows the flagellum (F) coiled on top of the cell body. The insert is an oriented slice showing the continuity between the nucleus (N) and the FAZ-associated reticulum (ER). Directions towards posterior and anterior ends of the cell are indicated with dashed white arrows. The white asterisk in the top left corner of each slice points out at crystalline ice. The scale bar represents 300 nm.

The FAZ filament appears as a succession of regularly spaced stick-like dark densities found close to the membrane of the cell body facing the flagellum (Fig. 1C, arrows). Using an oriented virtual tomographic slice, it is possible to better visualise the periodic pattern of these structures (Fig. 1C, insert). The lumen of the FAZ-associated reticulum is observed intracellularly next to the FAZ filament (Fig. 1C, ER). In an oriented virtual tomographic slice, a large part of the FAZ-associated reticulum is visible in continuity with the nucleus (Fig. 1D, insert). The flagellum coils along the outer surface of the

cell body (Fig. 1D). The visualisation of all these structures is possible since cryo-STET offers strong contrast and high tilt angles possibilities (e.g. greater than ±70°) even at such thickness (> 1µm). A movie has been generated to better appreciate the localisation of most of the above-mentioned elements in the cellular context (Movie 1).

Tight contact between cellular and flagellar membranes

We next focused on the space separating the cellular and the flagellar membranes in a cryo-tomogram collected at about 4 µm after the collar of a cell (Fig. 2). In the first slices of the reconstruction, membranes are extremely close to each other, appearing as a single membrane (Fig. 2A-B). Then, densities corresponding to the flagellar and the cellular membranes appear slightly separated in the next slices (Fig. 2C-F). When sticks of the FAZ filament are visible, membranes appear again as a single membrane (Fig. 2G-I). This membrane close proximity is systematically observed in all collected cryo-tomograms, whatever the location on the flagellum (n=6).

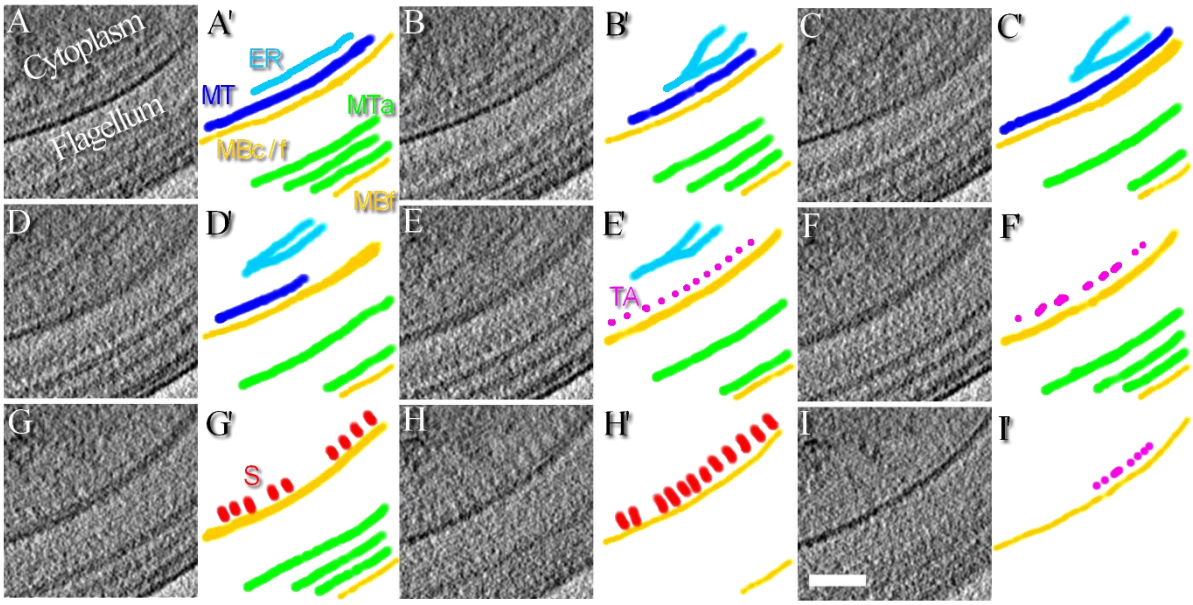

Figure 2. Organisation of the FAZ about 4µm after the collar. A-I) Images representing a continuous series of 14 nm-thick consecutive slices made through a tomographic reconstruction showing the structure of the flagellum/cell body interface at about 4 µm after the collar of a cell. A'–I') Next to each virtual slice, segmentation has been manually realised to highlight the various structures observed. Cellular and flagellum membranes (MBc and MBf, yellow), the FAZ-associated endoplasmic reticulum (ER, light blue), axonemal microtubules (MTa, green) and a microtubule (MT, dark blue) associated to stick-like structures of the FAZ (S, red) by thin appendages (TA, pink) are highlighted. The scale bar represents 150 nm.

In previous studies on resin-embedded *T. brucei* procyclic cells, flagellar and cellular membranes are separated by a few tens of nanometres (Sherwin and Gull, 1989). To rule out the fact that the difference might arise from cell stage differences, the comparative studies performed on samples from procyclic and bloodstream forms showed that both cell types display a similar gap between flagellar and cellular membranes (Buisson and Bastin, 2010). A similar gap is also observed in bloodstream forms of *T. brucei* (Vickerman, 1962), *T. evansi* (Hiruki, 1987) and *T. congolense* (Vickerman, 1969). Membrane structure is perturbed during sample preparation, especially when dehydration occurs, so further comparison is made with other works in which cells have been prepared and observed in cryo-conditions. Here, a 30 nm gap is observed between the flagellar and the cellular membranes of *T. brucei* procyclic cells (Höög et al., 2012). Since the work of Höög *et al.* has been performed on procyclic cells without chemical fixation, it is difficult to assess whether this discrepancy arises from specificities of *T. brucei* life cycle stage or sample preparation protocols. Nevertheless, it is

difficult to believe that aldehyde fixation as used in the present study, can lead to such effects on membrane distances, especially since other elements are structurally well conserved. Moreover, despite several attempts to freeze procyclic cells, they did not behave as good as the bloodstreams during freezing, membranes were often found broken.

The FAZ filament, a mainly cytoplasmic structure made of stick-like densities

Components of the FAZ can be observed in the cryo-tomogram collected 4 µm after the collar of a cell (Fig. 2). A microtubule (Fig. 2, MT, dark blue) is visible between the cellular membrane (Fig. 2, MBc, yellow) and the FAZ-associated reticulum (Fig. 2, ER, light blue). The proximity of the FAZ-associated reticulum indicates that this microtubule most probably belongs to the microtubule quartet. Sticks of the FAZ filament are present few slices deeper in the reconstruction (Fig. 2, S, red). It is worth noting that a succession of thin and punctuated structures (Fig. 2, TA, pink) is present on both sides of the FAZ filament sticks. The organisation of the FAZ filament, the FAZ-associated ER and a microtubule can also be accessed from a top-view orientation in a reconstruction of the anterior end of another cell (Suppl. 1). Sticks of the FAZ filament are ~30 nm-long cytoplasmic entities in contact with the membrane or anchored into it. After denoising of the data using an edge-enhancing noise-reduction anisotropic diffusion filter (Moreno et al., 2018), short densities in the flagellar compartment are sometimes facing cytoplasmic sticks (Fig. 3A, arrowheads).

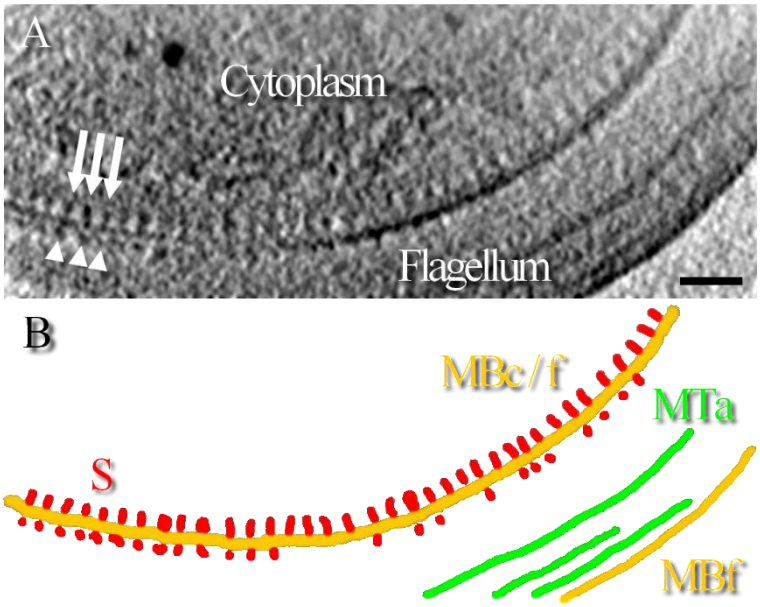

Figure 3. A tightly organised array of intracellular sticks and short flagellar densities. A) Oriented 14 nm-thick slice of a filtered reconstruction in which densities are visible on both sides of the cellular and flagellar membranes. Cytoplasmic sticks of the FAZ filament (white arrows) are longer and more regularly arranged than the flagellar densities facing them (white arrowheads). B) Manual segmentation of the cellular and flagellum membranes (MBc and MBf, yellow), axonemal microtubules (MTa, green), FAZ cytoplasmic stick-like structures (S, red) and FAZ flagellar short densities (red). The scale bar represents 150 nm.

In previous works, sticks of the FAZ filament are also described as cytoplasmic entities (Buisson and Bastin, 2010) and some thin fibrous densities are visible in the flagellar compartment (Sherwin and Gull, 1989). In conventional electron microscopy studies, dehydration of cells together with the use of contrasting agents might increase the visibility of these small structures. In tomography, the sample is not fully tilted inside the electron microscope during the data collection, creating a lack of information in the Fourier space (*i.e.* the missing wedge) which has the effect of blurring the 3D reconstruction in one direction. This missing wedge effect can also explain why, depending on the orientation of the cell, small flagellar densities are not consistently observed associated to the FAZ filament sticks. If electron

dose was not a limitation in cryo-STET, higher magnification tomographic studies would help better describing these thin flagellar structures.

Sticks are heterogeneously distributed along the FAZ filament

The first cryo-tomograms presented in this work describe the stick organisation at only some positions along the FAZ. To better characterise the stick distribution horizontally along the FAZ filament, several cryo-tomograms were collected at various locations in different uniflagellated cells in a systematic manner to cover most of the FAZ filament. Overall, six cryo-tomograms were collected, each representing about 2 to 3 µm-long portions of FAZ filament. Areas of interest are located at i) the exit of the flagellar pocket, ii) about 4 µm after the collar, iii) about 7 µm after the collar and iv) at the distal end of the FAZ filament (Fig. 4A). To better describe the most proximal and the most distal locations, two tomograms of each zone were collected. A table summarises the position of each tomogram and the figure(s) in which they are displayed (Suppl. Table 1). Based on the analysis of two different cells, no FAZ filament sticks are observed at the proximal region of the flagellum (*i.e.* from the collar up to the first micron of the axoneme) even though the FAZ-associated reticulum is visible (Suppl. 2). As observed above, at about 4 µm after the collar the sticks are present and form the regular array of the FAZ filament (Fig. 1-3). On the tomogram collected at about 7 µm after the collar, the curvature of the flagellum is less pronounced and the sticks form an almost straight array (Fig. 5 and Suppl. 3). Sticks were previously observed in a top-view orientation at the anterior tip of a cell (Suppl. 1). A second tomogram collected at the anterior end of another cell contains side-view orientation of sticks, confirming their presence at the most distal part of the FAZ (Suppl. 4).

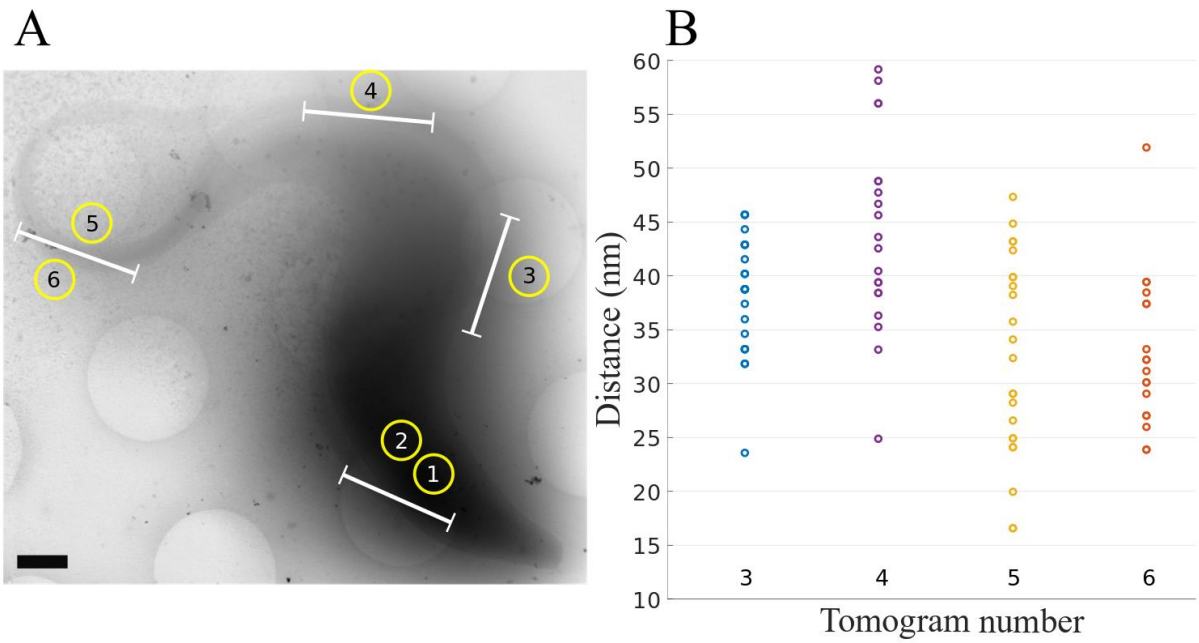

Figure 4. Localisation of investigated FAZ filament portions and measurement of the stick interdistance. Overall six cryo-tomograms were collected to search for the presence of sticks along the FAZ. The distance between two consecutive sticks is measured on the four cryo-tomograms in which sticks are observed. A) Cryo-STEM picture of a *T. brucei* bloodstream cell given as an example to show the positions where the six cryo-tomograms have been collected. For the sake of clarity, cryo-tomograms were collected on different cells. The FAZ portions analysed in each cryo-tomogram are represented by white bars. B) Plot showing the distribution of the stick interdistance for each tomogram in which sticks are observed. The number below each column represents the tomogram number as used in A. Scale bar is 700 nm.

In the literature, regularly arranged densities of the FAZ filament observed in electron microscopy are implicitly thought to correspond to FAZ filament proteins which have been detected by immunofluorescence. This association is particularly relevant for FAZ filament proteins that display a punctuated pattern in fluorescence. Following this idea, the absence of sticks at proximal locations as observed in the present study does not agree with immunofluorescence data in which most of the FAZ filament proteins were found to be present at equivalent proximal locations (Kohl et al., 1999; Moreira et al., 2017; Sunter et al., 2015; Vaughan et al., 2008). However, in the work of Moreira *et al.*, the signal of FAZ10 is weaker than that of FAZ1 at proximal locations (Moreira et al., 2017). Since FAZ10 is a giant protein (0.5 MDa) it is likely to have a significant contribution in the structure observed in electron microscopy. Its potential relative low abundance at most proximal regions of the FAZ filament might explain why sticks are not observed in the present study. Based on this hypothesis, higher magnification images might help identifying small protein complexes that would not contain FAZ10. Furthermore, since most of the immunofluorescence works were made on procyclic cells, it might also indicate differences in *T. brucei* cell stages that could be settled on with additional structural and molecular comparative studies.

To further analyse the organisation of the FAZ filament, systematic measurement of the distance between two consecutive sticks is performed (Fig. 4B). The overall mean distance is 37.0±8.5 nm (n=95, including all tomograms). The closest mean distance is observed at the distal end of the FAZ filament (32.4±9.3 nm, n=18) whereas the largest one is measured at about 7 µm after the collar (44.0±9.0 nm, n=20). One-way analysis of variance (ANOVA) shows that measurements are statistically different between these locations on the flagella (p-values ≤ 0.0055) indicating that FAZ filament sticks are not homogenously distributed. ANOVA also shows that the two measurements made at distal ends of FAZ filaments are not statistically different (p-value = 0.8784). These results are in agreement with the heterogeneous horizontal organisation of the FAZ filament stick. Measurement mean and standard deviation values as well as statistical test results are available as supplementary information (Suppl. 5).

Trypanosomes swim forward with the tip of the flagellum leading (Baron et al., 2007; Langousis and Hill, 2014; Walker, 1961). This is due to the fact that beating is initiated at the tip of the flagellum, the waveform being transmitted to the base of the flagellum. It makes sense that FAZ filament sticks are present in high density at the distal tip of the FAZ filament to efficiently attach the flagellum to the cell body during flagellum formation and in mature cells. The observation of FAZ filament sticks at the cell anterior tip is in agreement with the distal localisations of FAZ4, FAZ6, FAZ7, FAZ11 to FAZ14, TbSAS4 and TOEFAZ1 proteins (Hu et al., 2015; McAllaster et al., 2015; Sunter et al., 2015).

Thin appendages connect the FAZ to microtubules

As observed above in the cryo-tomogram collected about 4 µm after the collar, thin appendages are present between sticks of the FAZ filament and microtubules (Fig. 2, pink). Magnified views of the sticks and appendages are available as supplementary (Suppl. 6). To verify that appendages are present along the FAZ filament, all cryo-tomograms are investigated, including the one collected about 7 µm after the collar (Fig. 5). Thin appendages (Fig. 5, TA, pink) are visible on both sides of the sticks (Fig. 5, S, red). More slices of this 3D reconstruction are available as supplementary (Suppl. 3). Additional images show that the closest microtubule is not at a fixed distance of the sticks depending on which side of the sticks this microtubule is located. More precisely, the distance (about 40 nm) between sticks and the closest microtubule of the microtubule quartet is greater than the distance (about 20 nm) between sticks and the closest subpellicular microtubule.

During the exploration of the side-view cryo-tomogram collected at the anterior end of a *T. brucei* cell, it is not evident to identify FAZ-associated reticulum and microtubules (Suppl. 4). Indeed, because of a different molecular composition or because of the steric hindrance imposed by the very thin diameter at the cell anterior end (about 150 nm), the FAZ organisation is modified. In previously observed cryo-tomograms, the cell diameter could accommodate the entire FAZ in one single side of

the cell. When the cell diameter becomes very small, the FAZ might have to organise differently, most probably decorating the whole circumference of the cell, explaining why it is difficult to visualise all components. Nevertheless, thin appendages are present and clearly visible until the anterior tip of the cell body. Because of the small diameter of the cell body in this reconstruction, it is not possible to comment on the distance separating sticks and microtubules.

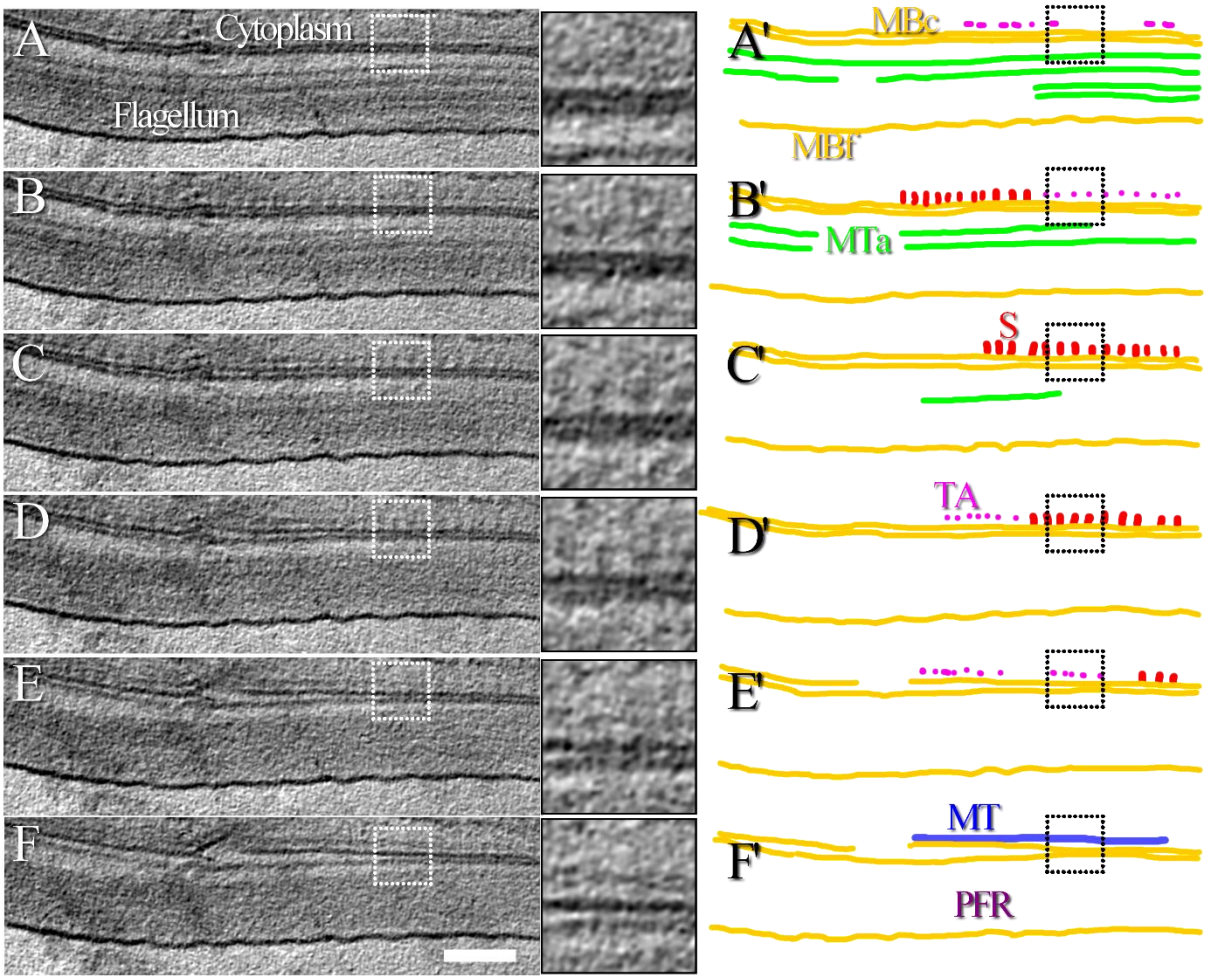

Figure 5. Thin appendages connect microtubules to the FAZ filament sticks. A-F) Continuous series of 10 nm-thick consecutive slices made through a tomographic reconstruction showing the structure of the FAZ filament at about 7 µm after the collar of a cell. Each insert represents a magnified view of the original image. The location of the insert is indicated by a dotted white square. A'-F') Segmentation highlighting the various structures observed in A-F. The cellular and flagellum membranes (MBc and MBf, yellow), the paraflagellar rod (PFR), the axonemal microtubules (MTa, green) and the microtubules (MT, blue) connected to stick-like structures of the FAZ (S, red) by thin appendages (TA, pink) are highlighted. The position of the inserts is indicated by the dotted black square. The scale bar represents 200 nm.

Based on the observation of three cryo-tomograms, representing over 6 µm of FAZ filament, thin appendages are consistently observed next to the sticks. These appendages represent the microtubule quartet microtubule to FAZ filament domain connection and the FAZ filament domain to subpellicular microtubule connection previously described (Sunter and Gull, 2016). Moreover, since their length varies between ~20 to ~40 nm depending on the side of the sticks they locate, this analysis is in favour of the existence of two connections of different nature, yet to be acknowledged. More resolute and detailed analysis is necessary to better describe these connections between FAZ filament sticks and microtubules.

Towards an identification of the stick nature and function

As mentioned above, the literature implicitly associates the regularly arranged densities of the FAZ filament observed in electron microscopy to the presence of FAZ filament proteins detected by immunofluorescence. To ascertain the identity of the proteins constituting the FAZ filament stick, a comparison is attempted between the structures observed in cryo-STET and predicted structures of FAZ filament proteins. To this purpose, manual measurements is carried out to better describe the stick structure. Their average width and height are 11.4±3.0 nm (n=56) and 34.2±7.2 nm (n=56), respectively (Suppl. 7). Current resolution does not allow to comment further on the cylindrical shape or the hollowness of the sticks.

Proteins whose localisation and dimensions could be compatible are examined (*i.e.* FAZ1 to FAZ3, FAZ5, FAZ8 to FAZ10 and CC2D) (Moreira et al., 2017; Sunter et al., 2015; Vaughan et al., 2008; Zhou et al., 2015, 2011). 3D structure prediction based on protein homology is carried out using Phyre2 (Kelley et al., 2015). Overall, six protein structures are predicted with high confidence (*i.e.* above 50% of the sequence modelled with more than 90% confidence) (Suppl. 8). The predicted structures of FAZ1, FAZ2, FAZ8, FAZ9, FAZ10 and CC2D include 10 nm-long (or more) domains mostly made of α-helices, fitting the dimensions of the FAZ filament sticks. More interestingly, domains structurally relevant with desmosome homology is predicted, among which dynein stalk and motor, kinesin stalk, desmoplakin and plakoglobin. The list of predicted relevant domains is available as supplementary (Suppl. 9).

A kinesin domain was found in FAZ7, which is present at the distal end of the FAZ filament (Sunter et al., 2015). Subpellicular microtubules have the right polarity for dynein motors to reach the distal end of the cell (Robinson et al., 1995). It is tempting to hypothesise that subpellicular microtubules are used as rails to guide and to extend the FAZ intracellularly. In the present study, the predicted presence of other dynein motor domains in FAZ1, FAZ2 and FAZ10 reinforces the possibility for such mechanism (Suppl. 9). Predicted homologies with kinesin and dynein stalk structures concurs with the hypothesis of functional dynein in FAZ filament proteins.

In the literature, the morphological resemblance between FAZ and desmosomes led to the search of proteins with compatible desmosomal structure or function. Bioinformatics analysis on whole *T. brucei* genome identified an armadillo repeat domain similar to that of desmosome proteins in FAZ9 (Sunter et al., 2015). In the present work, Phyre2 also predicted the presence of an armadillo repeat/plakoglobin domain in FAZ9 but also predicted a desmoplakin domain in FAZ1 and FAZ10 (Suppl. 9). Most interestingly, FAZ1 and FAZ9 were previously described as potential partners, in full agreement with a desmosome-like structure of the FAZ (Sunter and Gull, 2016).

The potential existence of such domains in FAZ proteins brings more material to elaborate the homology with desmosomes. The prediction of a desmoplakin domain and a dynein motor one in FAZ1 and FAZ10 would place the latter between cytoskeletal elements composed by subpellicular microtubules and the other FAZ proteins. More precisely, the protein FAZ9 and its predicted plakoglobin domain would be the most favourable partner of FAZ1 and FAZ10 (Fig. 6).

The corresponding growing model associated to this FAZ protein organisation would be relatively similar to the "*pull*" model (Sunter and Gull, 2016). Nevertheless, whereas the *"pull"* model involves the presence of a putative protein in the flagellar compartment to elongate the FAZ, the "*alternative pull*" model proposed herein only involves proteins already identified. The driving force of the FAZ elongation would originate from the force exerted by the predicted dynein motor domains of FAZ1 and FAZ10 (and perhaps FAZ2) on subpellicular microtubules (Fig. 6).

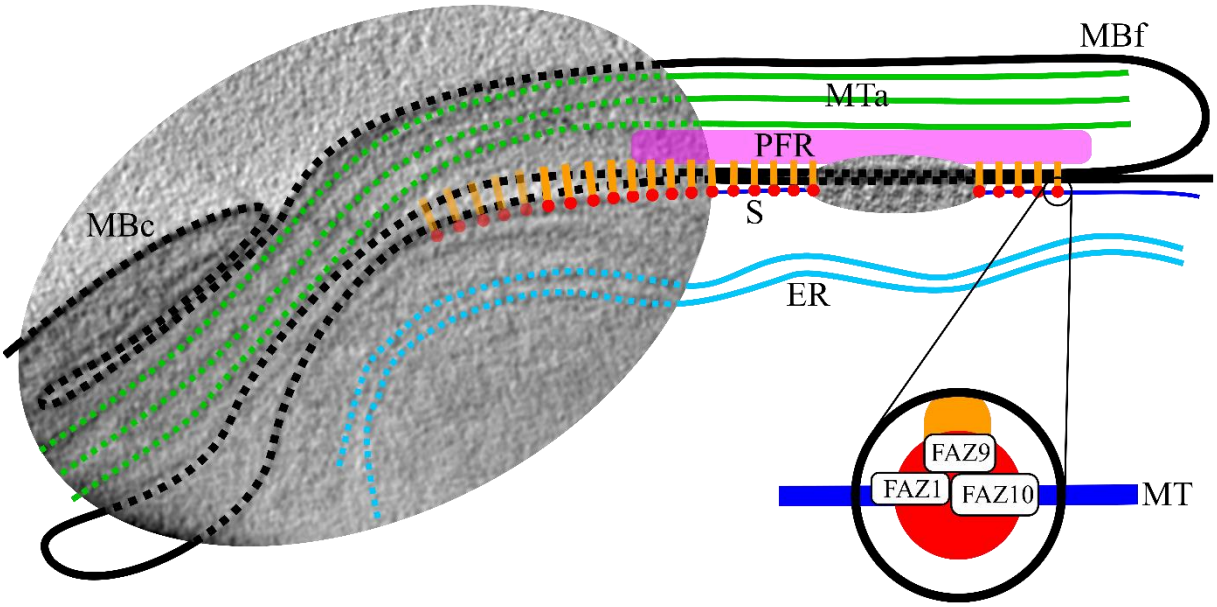

Figure 6. "*Alternative pull*" model of the FAZ elongation. The model is scaled on top of cryo-STET images. Several structures are drawn: cellular and flagellar membranes (MBc and MBf, respectively), the FAZ-associated reticulum (ER, light blue), the paraflagellar rod (PFR, pink), axonemal microtubules (MTa, green), the subpellicular microtubule (MT, dark blue) and FAZ filament sticks (S, red). The orange drawing represents the proteins connecting the cellular and flagellar membranes. Some structures are dotted when present on top a cryo-STET images for visual purposes. Some proximal orange and red structures are faded because their presence has not been confirmed by cryo-STET. The sticks are regularly placed following the pattern present in the cryo-STET image. The pulling mechanism is explained in the zoom-in of a stick. Predicted dynein motor domains of FAZ1 and FAZ10 enable connection with the subpellicular microtubule. Desmoplakin domains of FAZ1 and FAZ10 favour the connection with the plakoglobin domain of FAZ9. Connections with other FAZ filament partners allow the transport of the whole FAZ filament.

Conclusion

This work focus on the structural study of the FAZ filament organisation *in situ* in whole *T. brucei* cells using cryo-STET. The observation of typical, textbook-type, intracellular structures attests the good preservation of cell integrity during plunge-freezing. The capacity to investigate micrometre-thick cells permits the recovery of a vast and rich amount of structural information. This work confirms simulations on thickness limitation (Rez et al., 2016). Such 3D nanometric resolution allows the description of the heterogeneous organisation of FAZ filament sticks and the visualisation of thin appendages connecting FAZ filament sticks to neighbouring microtubules. The current study draws a broader 3D cryo-map of the FAZ filament updating what has previously been observed in conventional electron microscopy of thin sample sections.

The "*alternative pull*" model is based on i) the proximity observed between FAZ filament sticks and subpellicular microtubules, ii) the selection of FAZ filament proteins compatible with the stick dimensions and iii) the prediction of structural domains relevant in a desmosome-like environment. Mutations in the predicted dynein domains of FAZ1 and FAZ10, if they do not perturb the interactions with other FAZ filament proteins, should give a direct evidence of the role of these potential molecular motors in the FAZ filament assembly.

Now that important knowledge about FAZ proteins has been gathered and that "*a pattern has emerged linking the RNAi phenotype observed and protein localisation*" (Sunter and Gull, 2016), high resolution structural studies of RNAi phenotypes could extend our understanding of *T. brucei*

morphogenesis. Partially-detached flagella phenotype observed in FAZ1^{RNAi} and FAZ5^{RNAi} cell lines (Sunter et al., 2015) are characterised by a mixture of mature and incomplete FAZ structures. A direct structural comparison of these two states would certainly help understanding the complex FAZ organisation. One of the main challenges would be to produce these high resolution maps in a whole cellular environment. Cryo-focused ion beam associated to cryo-TET would most certainly be able to produce such high-resolution (Schaffer et al., 2015). However, if whole cells have to be kept, cryo-STET will be preferred. Currently, high resolution magnifications in cryo-STET are limited by the electron dose. Several strategies based on sparse acquisition exist to efficiently reduce the electron dose in STET but have only been applied to non-cryo samples (Trépout, 2019; Vanrompay et al., 2019). By combining such sparse data collection schemes and dedicated algorithm to reconstruct sparse data (Donati et al., 2017; Leary et al., 2013), greater magnifications would be allowed, thus improving the resolution currently available in cryo-STET.

Funding

This research was funded by two ANR grants (ANR-11-BSV8-016 and ANR-15-CE11-0002).

Acknowledgments

The author is greatly indebted to P. Bastin (Institut Pasteur, Paris, France) for making this study possible by giving access to the *T. brucei* material, for critical reading of the manuscript and for fruitful discussions about the biology of *T. brucei*. The author thanks C. Travaillé (Institut Pasteur, Paris, France) for providing *T. brucei* bloodstream samples. J.-P. Michel (Institut Galien Paris-Sud, Châtenay-Malabry, France) is acknowledged for his critical reading of the manuscript. The author acknowledges the PICT-IBiSA for providing access to the cryo-electron microscopy facility at Institut Curie Orsay.

Conflicts of Interest

The author declares no conflict of interest.

References

Aoyama, K., Takagi, T., Hirase, A., Miyazawa, A., 2008. STEM tomography for thick biological specimens. Ultramicroscopy 109, 70–80. https://doi.org/10.1016/j.ultramic.2008.08.005

Baron, D.M., Kabututu, Z.P., Hill, K.L., 2007. Stuck in reverse: loss of LC1 in Trypanosoma brucei disrupts outer dynein arms and leads to reverse flagellar beat and backward movement. Journal of Cell Science 120, 1513–1520. https://doi.org/10.1242/jcs.004846

Bastin, P., Sherwin, T., Gull, K., 1998. Paraflagellar rod is vital for trypanosome motility. Nature 391, 548. https://doi.org/10.1038/35300

Beneke, T., Madden, R., Makin, L., Valli, J., Sunter, J., Gluenz, E., 2017. A CRISPR Cas9 high-throughput genome editing toolkit for kinetoplastids. R Soc Open Sci 4. https://doi.org/10.1098/rsos.170095

Berriman, M., Ghedin, E., Hertz-Fowler, C., Blandin, G., Renauld, H., Bartholomeu, D.C., Lennard, N.J., Caler, E., Hamlin, N.E., Haas, B., Böhme, U., Hannick, L., Aslett, M.A., Shallom, J., Marcello, L., Hou, L., Wickstead, B., Alsmark, U.C.M., Arrowsmith, C., Atkin, R.J., Barron, A.J., Bringaud, F., Brooks, K., Carrington, M., Cherevach, I., Chillingworth, T.-J., Churcher, C., Clark, L.N., Corton, C.H., Cronin, A., Davies, R.M., Doggett, J., Djikeng, A., Feldblyum, T., Field, M.C., Fraser, A., Goodhead, I., Hance, Z., Harper, D., Harris, B.R., Hauser, H., Hostetler, J., Ivens, A., Jagels, K., Johnson, D., Johnson, J., Jones, K., Kerhornou, A.X., Koo, H., Larke, N., Landfear, S., Larkin, C., Leech, V., Line, A., Lord, A., Macleod, A., Mooney, P.J., Moule, S., Martin, D.M.A., Morgan, G.W., Mungall, K., Norbertczak, H., Ormond, D., Pai, G., Peacock, C.S., Peterson, J., Quail, M.A., Rabbinowitsch, E., Rajandream, M.-A., Reitter, C., Salzberg, S.L., Sanders, M., Schobel, S., Sharp, S., Simmonds, M., Simpson, A.J., Tallon, L., Turner, C.M.R., Tait, A., Tivey, A.R., Van Aken, S., Walker, D., Wanless, D., Wang, S., White, B., White, O., Whitehead, S., Woodward,

494 J., Wortman, J., Adams, M.D., Embley, T.M., Gull, K., Ullu, E., Barry, J.D., Fairlamb, A.H.,
495 Opperdoes, F., Barrell, B.G., Donelson, J.E., Hall, N., Fraser, C.M., Melville, S.E., El-Sayed,
496 N.M., 2005. The genome of the African trypanosome Trypanosoma brucei. Science 309, 416–
497 422. https://doi.org/10.1126/science.1112642
498 Blisnick, T., Buisson, J., Absalon, S., Marie, A., Cayet, N., Bastin, P., 2014. The intraflagellar transport
499 dynein complex of trypanosomes is made of a heterodimer of dynein heavy chains and of
500 light and intermediate chains of distinct functions. Mol Biol Cell.
501 https://doi.org/10.1091/mbc.E14-05-0961
502 Buisson, J., Bastin, P., 2010. Flagellum Structure and Function in Trypanosomes, in: de Souza, W.
503 (Ed.), Structures and Organelles in Pathogenic Protists. Springer Berlin Heidelberg, Berlin,
504 Heidelberg, pp. 63–86. https://doi.org/10.1007/978-3-642-12863-9_3
505 Büscher, P., Cecchi, G., Jamonneau, V., Priotto, G., 2017. Human African trypanosomiasis. Lancet 390,
506 2397–2409. https://doi.org/10.1016/S0140-6736(17)31510-6
507 Dean, S., Sunter, J., Wheeler, R.J., Hodkinson, I., Gluenz, E., Gull, K., 2015. A toolkit enabling efficient,
508 scalable and reproducible gene tagging in trypanosomatids. Open Biol 5, 140197.
509 https://doi.org/10.1098/rsob.140197
510 Donati, L., Nilchian, M., Trepout, S., Messaoudi, C., Marco, S., Unser, M., 2017. Compressed sensing
511 for STEM tomography. Ultramicroscopy 179, 47–56.
512 https://doi.org/10.1016/j.ultramic.2017.04.003
513 Frank, J. (Ed.), 2006. Electron Tomography: Methods for Three-Dimensional Visualization of
514 Structures in the Cell, 2nd ed. Springer-Verlag, New York.
515 Goddard, T.D., Huang, C.C., Meng, E.C., Pettersen, E.F., Couch, G.S., Morris, J.H., Ferrin, T.E., 2018.
516 UCSF ChimeraX: Meeting modern challenges in visualization and analysis. Protein Sci. 27, 14–
517 25. https://doi.org/10.1002/pro.3235
518 Heddergott, N., Krüger, T., Babu, S.B., Wei, A., Stellamanns, E., Uppaluri, S., Pfohl, T., Stark, H.,
519 Engstler, M., 2012. Trypanosome motion represents an adaptation to the crowded
520 environment of the vertebrate bloodstream. PLoS Pathog. 8, e1003023.
521 https://doi.org/10.1371/journal.ppat.1003023
522 Hiruki, T., 1987. Existence of a connecting system in the flagellar apparatus and the accessory
523 structures of Trypanosoma evansi. Zentralblatt für Bakteriologie, Mikrobiologie und Hygiene.
524 Series A: Medical Microbiology, Infectious Diseases, Virology, Parasitology 264, 392–398.
525 https://doi.org/10.1016/S0176-6724(87)80061-5
526 Höög, J.L., Bouchet-Marquis, C., McIntosh, J.R., Hoenger, A., Gull, K., 2012. Cryo-electron tomography
527 and 3-D analysis of the intact flagellum in Trypanosoma brucei. J Struct Biol 178, 189–198.
528 https://doi.org/10.1016/j.jsb.2012.01.009
529 Hu, H., Zhou, Q., Li, Z., 2015. SAS-4 Protein in *Trypanosoma brucei* Controls Life Cycle Transitions by
530 Modulating the Length of the Flagellum Attachment Zone Filament. J. Biol. Chem. 290,
531 30453–30463. https://doi.org/10.1074/jbc.M115.694109
532 Kelley, L.A., Mezulis, S., Yates, C.M., Wass, M.N., Sternberg, M.J.E., 2015. The Phyre2 web portal for
533 protein modeling, prediction and analysis. Nat Protoc 10, 845–858.
534 https://doi.org/10.1038/nprot.2015.053
535 Kohl, L., Robinson, D., Bastin, P., 2003. Novel roles for the flagellum in cell morphogenesis and
536 cytokinesis of trypanosomes. EMBO J. 22, 5336–5346.
537 https://doi.org/10.1093/emboj/cdg518
538 Kohl, L., Sherwin, T., Gull, K., 1999. Assembly of the paraflagellar rod and the flagellum attachment
539 zone complex during the Trypanosoma brucei cell cycle. J. Eukaryot. Microbiol. 46, 105–109.
540 Koyfman, A.Y., Schmid, M.F., Gheiratmand, L., Fu, C.J., Khant, H.A., Huang, D., He, C.Y., Chiu, W.,
541 2011. Structure of Trypanosoma brucei flagellum accounts for its bihelical motion. Proc Natl
542 Acad Sci U S A 108, 11105–11108. https://doi.org/10.1073/pnas.1103634108
543 Kremer, J.R., Mastronarde, D.N., McIntosh, J.R., 1996. Computer visualization of three-dimensional
544 image data using IMOD. J Struct Biol 116, 71–6. https://doi.org/10.1006/jsbi.1996.0013

545 Lacomble, S., Vaughan, S., Gadelha, C., Morphew, M.K., Shaw, M.K., McIntosh, J.R., Gull, K., 2010.
546 Basal body movements orchestrate membrane organelle division and cell morphogenesis in
547 Trypanosoma brucei. J Cell Sci 123, 2884–91. https://doi.org/10.1242/jcs.074161
548 Lacomble, S., Vaughan, S., Gadelha, C., Morphew, M.K., Shaw, M.K., McIntosh, J.R., Gull, K., 2009.
549 Three-dimensional cellular architecture of the flagellar pocket and associated cytoskeleton in
550 trypanosomes revealed by electron microscope tomography. J Cell Sci 122, 1081–90.
551 https://doi.org/10.1242/jcs.045740
552 Langousis, G., Hill, K.L., 2014. Motility and more: the flagellum of Trypanosoma brucei. Nat Rev
553 Microbiol 12, 505–518. https://doi.org/10.1038/nrmicro3274
554 Leary, R., Saghi, Z., Midgley, P.A., Holland, D.J., 2013. Compressed sensing electron tomography.
555 Ultramicroscopy 131, 70–91. https://doi.org/10.1016/j.ultramic.2013.03.019
556 Lin, J., Nicastro, D., 2018. Asymmetric distribution and spatial switching of dynein activity generates
557 ciliary motility. Science 360. https://doi.org/10.1126/science.aar1968
558 Lin, J., Okada, K., Raytchev, M., Smith, M.C., Nicastro, D., 2014. Structural mechanism of the dynein
559 powerstroke. Nat Cell Biol 16, 479–485. https://doi.org/10.1038/ncb2939
560 Lucic, V., Leis, A., Baumeister, W., 2008. Cryo-electron tomography of cells: connecting structure and
561 function. Histochem Cell Biol 130, 185–96.
562 Lucic, V., Rigort, A., Baumeister, W., 2013. Cryo-electron tomography: the challenge of doing
563 structural biology in situ. J Cell Biol 202, 407–19. https://doi.org/10.1083/jcb.201304193
564 Mastronarde, D.N., Held, S.R., 2017. Automated tilt series alignment and tomographic reconstruction
565 in IMOD. J Struct Biol 197, 102–113. https://doi.org/10.1016/j.jsb.2016.07.011
566 McAllaster, M.R., Ikeda, K.N., Lozano-Núñez, A., Anrather, D., Unterwurzacher, V., Gossenreiter, T.,
567 Perry, J.A., Crickley, R., Mercadante, C.J., Vaughan, S., de Graffenried, C.L., 2015. Proteomic
568 identification of novel cytoskeletal proteins associated with TbPLK, an essential regulator of
569 cell morphogenesis in Trypanosoma brucei. Mol Biol Cell 26, 3013–3029.
570 https://doi.org/10.1091/mbc.E15-04-0219
571 Midgley, P.A., Weyland, M., 2003. 3D electron microscopy in the physical sciences: the development
572 of Z-contrast and EFTEM tomography. Ultramicroscopy 96, 413–31.
573 https://doi.org/10.1016/S0304-3991(03)00105-0
574 Moreira, B.P., Fonseca, C.K., Hammarton, T.C., Baqui, M.M.A., 2017. Giant FAZ10 is required for
575 flagellum attachment zone stabilization and furrow positioning in Trypanosoma brucei. J.
576 Cell. Sci. 130, 1179–1193. https://doi.org/10.1242/jcs.194308
577 Moreno, J.J., Martínez-Sánchez, A., Martínez, J.A., Garzón, E.M., Fernández, J.J., 2018. TomoEED: fast
578 edge-enhancing denoising of tomographic volumes. Bioinformatics 34, 3776–3778.
579 https://doi.org/10.1093/bioinformatics/bty435
580 Morriswood, B., Havlicek, K., Demmel, L., Yavuz, S., Sealey-Cardona, M., Vidilaseris, K., Anrather, D.,
581 Kostan, J., Djinović-Carugo, K., Roux, K.J., Warren, G., 2013. Novel Bilobe Components in
582 Trypanosoma brucei Identified Using Proximity-Dependent Biotinylation. Eukaryot Cell 12,
583 356–367. https://doi.org/10.1128/EC.00326-12
584 Ngô, H., Tschudi, C., Gull, K., Ullu, E., 1998. Double-stranded RNA induces mRNA degradation in
585 Trypanosoma brucei. Proc. Natl. Acad. Sci. U.S.A. 95, 14687–14692.
586 https://doi.org/10.1073/pnas.95.25.14687
587 Pennycook, S.J., Nellist, P.D., 2011. Scanning Transmission Electron Microscopy. Springer New York,
588 New York, NY.
589 Rez, P., Larsen, T., Elbaum, M., 2016. Exploring the theoretical basis and limitations of cryo-STEM
590 tomography for thick biological specimens. J Struct Biol 196, 466–478.
591 https://doi.org/10.1016/j.jsb.2016.09.014
592 Robinson, D.R., Sherwin, T., Ploubidou, A., Byard, E.H., Gull, K., 1995. Microtubule polarity and
593 dynamics in the control of organelle positioning, segregation, and cytokinesis in the
594 trypanosome cell cycle. J. Cell Biol. 128, 1163–1172. https://doi.org/10.1083/jcb.128.6.1163

595 Rotureau, B., Blisnick, T., Subota, I., Julkowska, D., Cayet, N., Perrot, S., Bastin, P., 2014. Flagellar
596 adhesion in Trypanosoma brucei relies on interactions between different skeletal structures
597 in the flagellum and cell body. J Cell Sci 127, 204–15. https://doi.org/10.1242/jcs.136424
598 Rotureau, B., Van Den Abbeele, J., 2013. Through the dark continent: African trypanosome
599 development in the tsetse fly. Front Cell Infect Microbiol 3.
600 https://doi.org/10.3389/fcimb.2013.00053
601 Satir, P., 1968. STUDIES ON CILIA. J Cell Biol 39, 77–94.
602 Schaffer, M., Engel, B.D., Laugks, T., Mahamid, J., Plitzko, J.M., Baumeister, W., 2015. Cryo-focused
603 Ion Beam Sample Preparation for Imaging Vitreous Cells by Cryo-electron Tomography. Bio
604 Protocol 5, 1575. https://doi.org/10.21769/BioProtoc.1575
605 Schneider, C.A., Rasband, W.S., Eliceiri, K.W., 2012. NIH Image to ImageJ: 25 years of image analysis.
606 Nat Methods 9, 671–5. https://doi.org/10.1038/nmeth.2089
607 Sherwin, T., Gull, K., 1989. The cell division cycle of Trypanosoma brucei brucei: timing of event
608 markers and cytoskeletal modulations. Philos. Trans. R. Soc. Lond., B, Biol. Sci. 323, 573–588.
609 https://doi.org/10.1098/rstb.1989.0037
610 Sistrom, M., Evans, B., Bjornson, R., Gibson, W., Balmer, O., Mäser, P., Aksoy, S., Caccone, A., 2014.
611 Comparative Genomics Reveals Multiple Genetic Backgrounds of Human Pathogenicity in the
612 Trypanosoma brucei Complex. Genome Biol Evol 6, 2811–2819.
613 https://doi.org/10.1093/gbe/evu222
614 Sousa, A.A., Leapman, R.D., 2012. Development and application of STEM for the biological sciences.
615 Ultramicroscopy 123, 38–49. https://doi.org/10.1016/j.ultramic.2012.04.005
616 Sun, S.Y., Kaelber, J.T., Chen, M., Dong, X., Nematbakhsh, Y., Shi, J., Dougherty, M., Lim, C.T., Schmid,
617 M.F., Chiu, W., He, C.Y., 2018. Flagellum couples cell shape to motility in Trypanosoma
618 brucei. Proc Natl Acad Sci U S A 115, E5916–E5925.
619 https://doi.org/10.1073/pnas.1722618115
620 Sunter, J.D., Gull, K., 2016. The Flagellum Attachment Zone: 'The Cellular Ruler' of Trypanosome
621 Morphology. Trends in Parasitology 32, 309–324. https://doi.org/10.1016/j.pt.2015.12.010
622 Sunter, J.D., Varga, V., Dean, S., Gull, K., 2015. A dynamic coordination of flagellum and cytoplasmic
623 cytoskeleton assembly specifies cell morphogenesis in trypanosomes. J Cell Sci 128, 1580–
624 1594. https://doi.org/10.1242/jcs.166447
625 Trépout, S., 2019. Tomographic Collection of Block-Based Sparse STEM Images: Practical
626 Implementation and Impact on the Quality of the 3D Reconstructed Volume. Materials
627 (Basel) 12. https://doi.org/10.3390/ma12142281
628 Vanrompay, H., Béché, A., Verbeeck, J., Bals, S., 2019. Experimental Evaluation of Undersampling
629 Schemes for Electron Tomography of Nanoparticles. Part. Part. Syst. Charact. 1900096.
630 https://doi.org/10.1002/ppsc.201900096
631 Vaughan, S., Kohl, L., Ngai, I., Wheeler, R.J., Gull, K., 2008. A Repetitive Protein Essential for the
632 Flagellum Attachment Zone Filament Structure and Function in Trypanosoma brucei. Protist
633 159, 127–136. https://doi.org/10.1016/j.protis.2007.08.005
634 Vickerman, K., 1969. The Fine Structure of Trypanosoma congolense in Its Bloodstream Phase. The
635 Journal of Protozoology 16, 54–69. https://doi.org/10.1111/j.1550-7408.1969.tb02233.x
636 Vickerman, K., 1962. The mechanism of cyclical development in trypanosomes of the Trypanosoma
637 brucei sub-group: An hypothesis based on ultrastructural observations. Transactions of the
638 Royal Society of Tropical Medicine and Hygiene 56, 487–495. https://doi.org/10.1016/0035-
639 9203(62)90072-X
640 Walker, P.J., 1961. Organization of function in trypanosome flagella. Nature 189, 1017–1018.
641 https://doi.org/10.1038/1891017a0
642 Wolf, S.G., Elbaum, M., 2019. CryoSTEM tomography in biology. Methods Cell Biol. 152, 197–215.
643 https://doi.org/10.1016/bs.mcb.2019.04.001
644 Wolf, S.G., Houben, L., Elbaum, M., 2014. Cryo-scanning transmission electron tomography of
645 vitrified cells. Nat Methods 11, 423–8. https://doi.org/10.1038/nmeth.2842

646 Wolf, S.G., Mutsafi, Y., Dadosh, T., Ilani, T., Lansky, Z., Horowitz, B., Rubin, S., Elbaum, M., Fass, D.,
647 2017. 3D visualization of mitochondrial solid-phase calcium stores in whole cells. eLife 6.
648 https://doi.org/10.7554/eLife.29929
649 Zhou, Q., Hu, H., He, C.Y., Li, Z., 2015. Assembly and maintenance of the flagellum attachment zone
650 filament in Trypanosoma brucei. J Cell Sci 128, 2361–2372.
651 https://doi.org/10.1242/jcs.168377
652 Zhou, Q., Liu, B., Sun, Y., He, C.Y., 2011. A coiled-coil- and C2-domain-containing protein is required
653 for FAZ assembly and cell morphology in Trypanosoma brucei. J Cell Sci 124, 3848–3858.
654 https://doi.org/10.1242/jcs.087676
655